Journal of Innovative Optical Health Sciences
Vol. 8, No. 5 (2015) 1550015 (10 pages)

DOI: 10.1142/S1793545815500157

A computer-based image analysis for tear ferning featuring

Ali S. Saad*,‡, Gamal A. El-Hiti† and Ali M. Masmali†
*Department of Biomedical Technology
College of Applied Medical Sciences
King Saud University, P. O. Box 10219
Riyadh 11433, Saudi Arabia
†Cornea Research Chair (CRC), Department of Optometry
College of Applied Medical Sciences, King Saud University
Riyadh 11433, Saudi Arabia
‡alisaad@ksu.edu.sa

Received 16 September 2014
Accepted 14 October 2014
Published 14 November 2014

The present work focuses on the development of a novel computer-based approach for tear ferning (TF) featuring. The original TF images of the recently developed five-point grading scale have been used to assign a grade for any TF image automatically. A vector characteristic (VC) representing each grade was built using the reference images. A weighted combination between features selected from textures analysis using gray level co-occurrence matrix (GLCM), power spectrum (PS) analysis and linear specificity of the image were used to build the VC of each grade. A total of 14 features from texture analysis were used. PS at different frequency points and number of line segments in each image were also used. Five features from GLCM have shown significant differences between the recently developed grading scale images which are: angular second moment at 0° and 45°, contrast, and correlation at 0° and 45°; these five features were all included in the characteristic vector. Three specific power frequencies were used in the VC because of the discrimination power. Number of line segments was also chosen because of dissimilarities between images. A VC for each grade of TF reference images was constructed and was found to be significantly different from each other's. This is a basic and fundamental step toward an automatic grading for computer-based diagnosis for dry eye.

Keywords: Objective grading; tear ferning new grading scale; texture analysis; image processing; PS.

‡Corresponding author.

1. Introduction

Tears production is very important for clear vision and eye health. Dry eye patients suffer from discomfort such as sensitivity to light, stinging, burning, blurriness, grittiness, or scratchy and itchy eye.[1–3] Such experiences could arise from the ocular surface due to changes in the quantity and quality of the overlaying tears. The multiple causes of dry eye make its diagnoses and treatment difficult.[4] Moreover, the currently available methods for the dry eye diagnosis are far from perfection.[5]

Different tear film quality and quantity tests are available and used daily in the clinic, such as, Schirmer's test,[6] phenol red thread test,[6] Rose Bengal staining,[7] tear break-up time (TBUT),[8] tear meniscus measurement,[9] and tear osmolarity.[10–12] The tear ferning (TF) test, which is simple and inexpensive[13] and can be used to examine the quality of the ocular tear film, has showed good specificity and sensitivity.[14] When a tear sample is allowed to dry on a glass slide under normal room temperature and humidity, different crystal ferning patterns can be observed under light microscopy. In 1984, Rolando suggested a four-type TF grading scale (types I–IV) in which types I and II were more often observed in normal eye subjects, and types III and IV were observed in dry eye patients.[15] Various other TF grading scales have been introduced since then,[16,17] however the Rolando TF grading scale remains the most commonly used in terms of popularity[18] and repeatability.[19]

Recently, a new five-point TF grading scale (Fig. 1) was developed,[20] to overcome some of the limitations associated with Rolando grading scale[13] such as poor differentiation between types I and II. The recently developed grading scale is capable of differentiating between TF grading patterns and can be used as a support for other dry eye tests.[20]

The present study is aimed toward the development of an automatic objective grading of TF

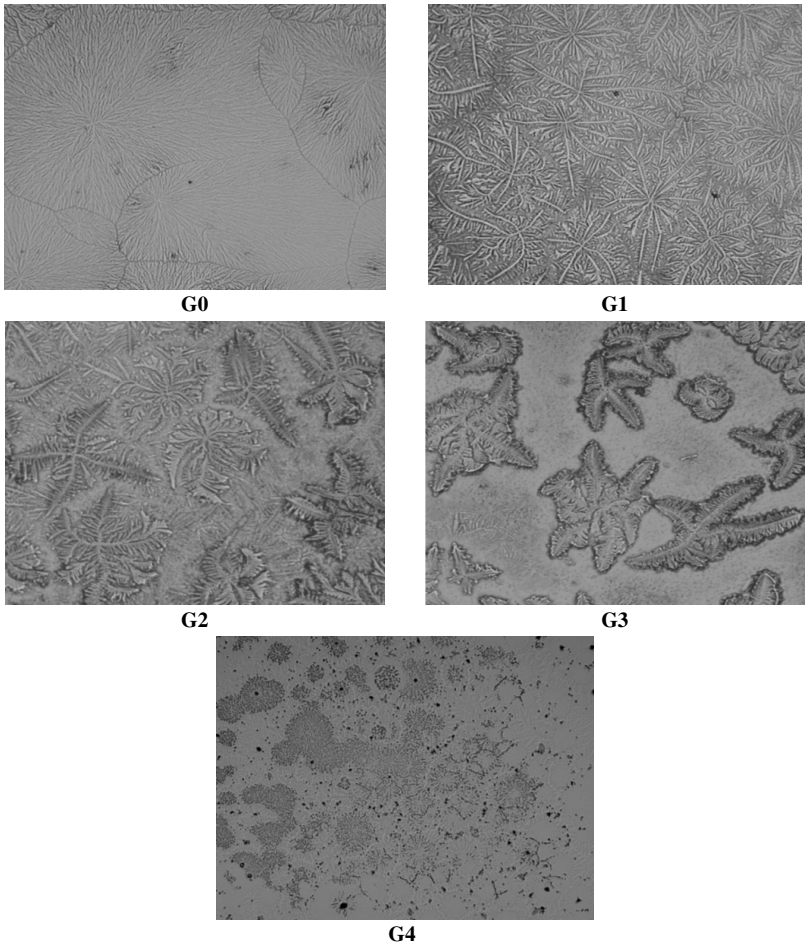

Fig. 1. The recently developed TF grading scale (grades 0–4).[20]

images to assign a grade to a TF image using features extracted from the image itself. The features are grouped into characteristics vector and compared to pre-constructed feature vectors of reference graded images of TF.

There have been many studies in solving classification problem based on various types of features and different methods of feature extraction.[21–23] Most of the features are generally obtained from texture by the application of a local operator, statistical analysis, or measurement in a transformed domain.[24] Gray level co-occurrence matrix (GLCM) is one of the earliest methods for the texture feature extraction proposed by Haralick *et al.*[25] in 1973 and remains as an important feature extraction method in the domain of texture analysis. A total of 14 features were extracted by Haralick from the GLCMs to characterize texture.[26] Many quantitative measures of texture are found in the literature.[27–30] Recently, special multi-dimensional co-occurrence matrices were used for object recognition and matching.[31–33] Dacheng *et al.*[34] used 3D co-occurrence matrices in content-based image retrieval (CBIR) applications.

The PS is an important tool to encode structural information. It gives global information about the basic elements that form the image. The power spectra of real-world images exhibit very different energy distributions for each orientations and spatial frequencies. In analyzing images from a wide set of real-world environments, a strong bias toward horizontal and vertical orientation are observed.[35] PS is also used for texture classification.[36] For this reason, PS is considered here for classification and was used for image registration and watermarking recently.[37] Here, we are not interested in a detailed analysis of the PS which would be as complicated as studying the pixelated image itself. For our application, the PS of the five-grade scale images has discriminative features at different frequency ranges. In this paper, the proposed VCs of grade image is a weighted combination between features from GLCM, PS, and linear specificity of the image.

2. Materials and Methods

The five reference images (Fig. 1) of the new grading scale[20] were used in our experimental study. In order to distinguish between grades, specific observations have been made to the images representing them. An observation is related to the frequency

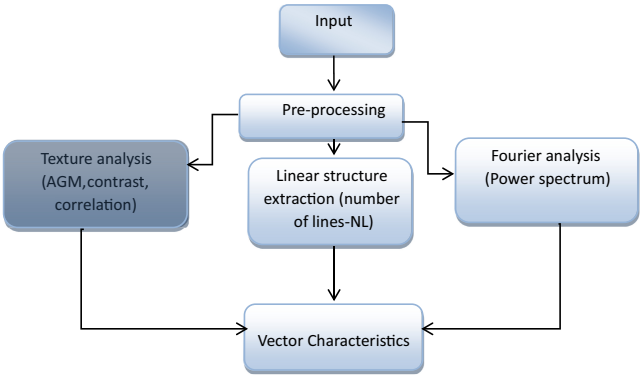

Fig. 2. Block diagram of the image processing scheme.

domain of the images, small details are more present in the low-grade images which represent in the frequency domain a high-frequency component in the Fourier space. The second observation is the more frequent presence of a line segment in the lower grades more than the higher ones. The third is the presence of different textures in the images representing each grade. For these reasons, we propose VCs combining all three observations; it includes texture analysis, linear structure analysis in time domain, and PS analysis in Fourier space. Figure 2 shows the block diagram of the method used for the construction of the VC.

All technical processing of digital images was made using ImageJ NIH software and Matlab 7. The following section describes each component method of VCs construction.

2.1. *Preprocessing of the original images*

In order to process the images, they should all be normalized to the same range of gray values and represented at similar conditions in terms of contrast and histogram distribution. In order to do so, a contrast enhancement procedure of the images was performed. It involves normalization and then histogram equalization. Figure 3 shows the images after contrast enhancement.

2.2. *Analysis of the images in time domain for linear structure detection*

The images were made into binaries before the analysis. This process was automatic and used the histogram of the image in order to group all pixels in

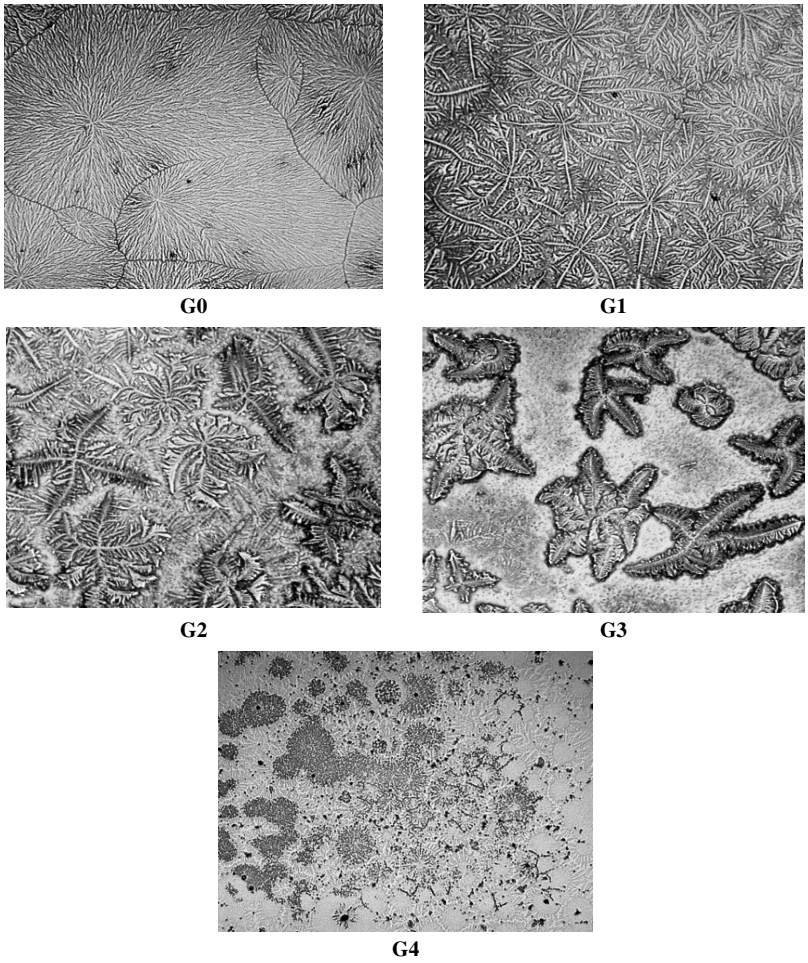

Fig. 3. Images after normalization and contrast enhancement.

the image into two groups. A threshold was selected from the histogram representing the global minimum. The values of all pixels having higher values than the threshold are set to 1 and those having values lower than the threshold are set to zero. Different types of automatic threshold exist in "ImageJ", all of them were tested on the original images and the "Outsu" method of threshold gave the optimal threshold for binarization. The images after the binarization process are shown in Fig. 4.

Particle analysis was used in order to differentiate between the grades in terms of linearity. This analysis counts and extracts the linear objects in the image. All objects less than 20 pixels in size were considered as noise. Objects were considered as lines if the circularity was close to zero (0.0–0.2). The outline of the detected objects and the number of linear objects (NL) detected in each image of grade 0 are shown in the results section.

2.3. *PS analysis*

In order to validate the observation related to the images' frequency distribution, the images were transformed into Fourier space using Fast Fourier Transform (FFT). The FFT for the grade 0 image is shown in Fig. 5. The 2D Fourier transform of digital image is given in Eq. (1) and the PS is given in Eq. (2).

$$Y_p[f_x, f_y] = \sum_{x=-\infty}^{\infty} \sum_{y=-\infty}^{\infty} g[x, y] \mathrm{e}^{-j2\pi(xf_x+yf_y)}, \quad (1)$$

$$P(f_x f_y) = |Y(f_x, f_y)|^2, \quad (2)$$

where, Y_P is the Fourier transform function; f_x, f_y are frequencies in the x and y directions. x, y are coordinates in real space; $g[x, y]$ represents a pixel of the image in real space; j is a complex number.

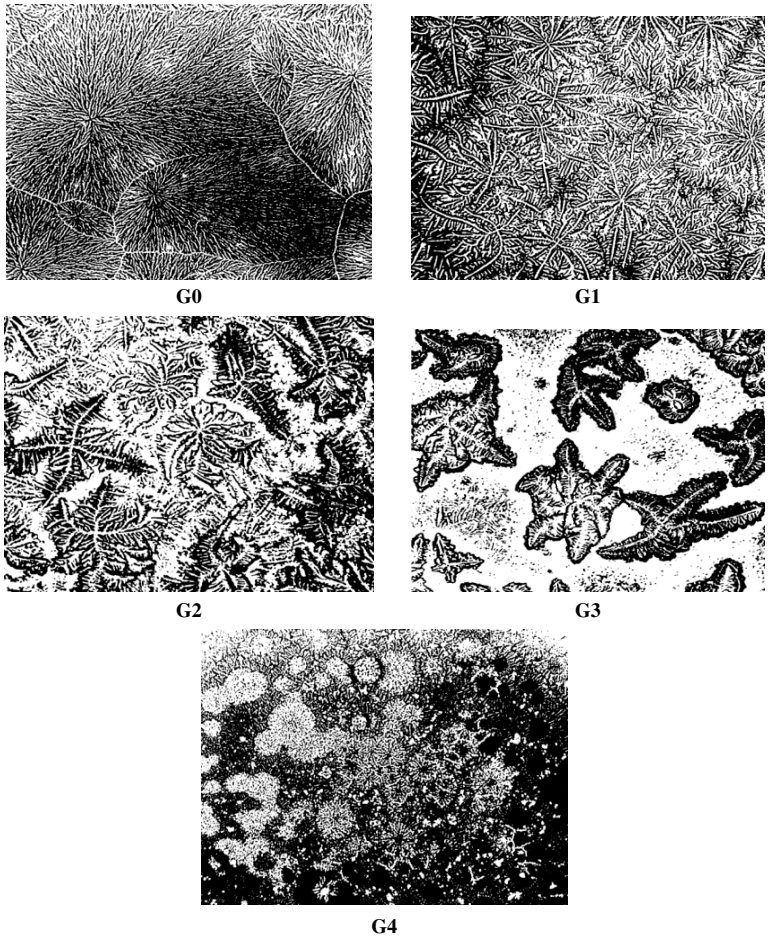

Fig. 4. Binary images.

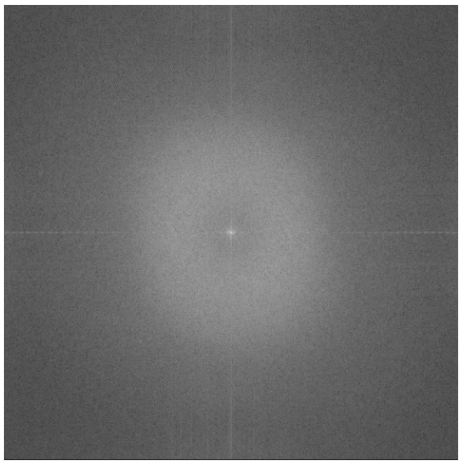

Fig. 5. The FFT for the grade 0 TF image.

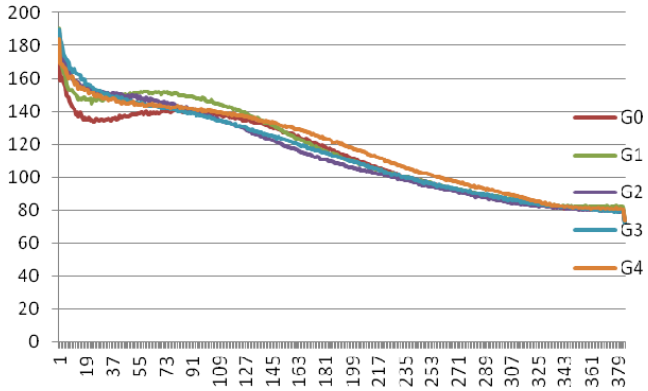

Fig. 6. The Radial plots of PS for five-grade scale images.

A visual analysis of the PS image was very difficult; in order to make the process of comparison easier in Fourier space a circularly averaged radial plot of the PS of each image was plotted as shown in Fig. 6.

2.4. *Texture analysis*

Texture analysis is an important tool for image classification. Features computed from the co-occurrence matrix are an efficient tools used to represent, compare, and classify textures. Co-occurrence matrix captures features of a texture using spatial

relations of similar gray tones. The following set of standard features derivable from a normalized co-occurrence matrix was used in this process in order to discover similarities and diversities in the grade images. The set include of standard features include angular 2nd moment [Eq. (3)], contrast [Eq. (4)], correlation [Eq. (5)], and entropy [Eq. (6)].

$$\text{Angular 2nd Moment (AGM)} = \sum_i \sum_j P[i,j]^2, \tag{3}$$

$$\text{contrast} = \sum_{n=0}^{Ng-1} n^2 \sum_{i=1}^{Ng} \sum_{j=1}^{Ng} P[i,j], \tag{4}$$

$$\text{where } |i-j| = n$$

$$\text{correlation} = \frac{\sum_{i=1}^{Ng} \sum_{j=1}^{Ng} (i,j) P[i,j] - \mu x \mu y}{\sigma x \sigma y}, \tag{5}$$

$$\text{Entropy} = -\sum_i \sum_j P[i,j] \log(P[i,j]), \tag{6}$$

where, $P[i,j]$ is the $[i,j]$th entry in a gray-tone spatial dependence matrix, Ng is the number of distinct gray levels in the quantized image, σ is the standard deviation and μ is the average.

One negative aspect of the co-occurrence matrix is that the extracted features do not necessarily correspond to visual perception. All the features were measured in 4 directions such as 0°, 45°, 90° and 135° by using a distance of 1 pixel.

3. Results

3.1. *PS analysis*

Figure 5 shows the FFT of the image of grade 0. Figure 6 shows the radial average PS of all TF grade images. At low frequency, area less than 30 Hz graded 0 to 3 were ranked from least to the greatest. Grade 4 in the low-frequency region was similar to grade 2. Figure 7 shows the PS for the first 4 grades (G0–G3). It was noticed that the power spectra between points 1 and 30 Hz for grades 0 to 3 were well ranked from the lowest to the highest. Grade 1 is dominant from point 43 up to 132 Hz then G4 dominates the PS up to 340 Hz. Ignoring G4, it was clear that G0 has the highest power in the range of 153–228 Hz, followed by G1, G3 and G2. Grades 0 to 3, which have patterns like trees branches, are ordered from the least to the greatest at low frequencies (3 to 30 Hz). Also, they were ordered from high to low power from G0 to G3 at high frequency from 153 to 228 Hz. From 228 to 380 Hz, all 4 grades have similar PS and G4 has a dominant PS from frequency of 132 to 340 Hz.

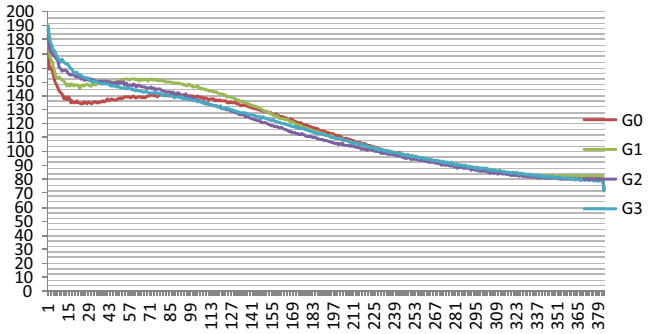

Fig. 7. PS of the images of grades 0, 1, 2, 3.

3.2. *Texture analysis*

The texture analysis is shown in Tables 1 and 2, where the values of four standard features selected were presented at different angles (0°, 90°, 45° and 135°). The distance used to calculate the features was 1 pixel. After examining the results in Tables 1 and 2, the entropy was eliminated because of the non-significant discrimination between the grade images. The correlation in Table 1 showed that the lowest value was for G0 and the highest was for the image of grade 3. Grades 1 and 2 were similar with a

Table 1. The texture features at angels 0° and 90°.

Gray level (0° and 90°)	AGM	Contrast	Correlation	Entropy
G0	0.57	0.135	0.63	0.93
G1	0.18	0.30	0.79	0.85
G2	0.32	0.16	0.79	0.92
G3	0.36	0.135	0.87	0.93
G4	0.33	0.24	0.70	0.88

Table 2. The texture features at angles 45° and 135°.

Gray level (45° and 135°)	AGM	Contrast	Correlation	Entropy
G0	0.39	0.11	0.98	0.96
G1	0.29	0.215	0.97	0.92
G2	0.32	0.12	0.98	0.95
G3	0.34	0.11	0.98	0.96
G4	0.33	0.16	0.97	0.93

value of 0.79. The correlation at direction 45° and 135° were not considered because of the similarity between the values of all grade reference images.

It was clear from Table 2 that G0 had the highest AGM (0.57), and the lowest AGM (0.18) was for G1. The AGM for G2 to G4 images was about 0.33. The highest contrast (0.3) was for G2 and the lowest was for G0 and G3 (0.135). The contrast of G4 was double as for G0 and G3. From Table 2, the same conclusion has been drawn as from Table 1, where G2, G3 and G4 have similar AGMs at different orientations (angles). Regarding the contrast, G1 in all orientations has the highest value followed by the value of G4.

3.3. *Linear structure analysis*

After applying the particle analysis function described in the method for detecting the lines or linear structures in the image, a graphical result was presented in Fig. 8. It shows a visual distribution of line segments in the images. Table 3 shows the number of lines (NBL) detected in each of the five grades images.

Table 3. The NBL detected in grades images.

Grade	NBL
Grade 0	185
Grade 1	85
Grade 2	24
Grade 3	24
Grade 4	68

3.4. *Proposed VC of the grade images*

From the resultant quantification of the observations described in previous sections, a careful selection of the components, especially those varying from one image to another, was performed. The selected components forming the proposed VC are shown in Eq. (7).

$$\mathrm{VC} = [\mathrm{PS}(19), \mathrm{PS}(80), \mathrm{PS}(190), \mathrm{NBL}, \mathrm{AGM0}, \mathrm{AGM45}, \mathrm{CORR0}, \mathrm{CON0}, \mathrm{CON45}], \quad (7)$$

where, PS(19) is the PS at low frequency at 19 Hz in the radial plot; PS(80) is the PS at medium frequency at 80 Hz in the radial plot; PS(190) is the PS at high frequency at pixel 190 in the radial plot; NBL is the NBL detected in the image; AGM0 is the angular moment at direction 0°; AGM45 is the angular moment at direction 45°; CORR0 is the correlation at direction 0°; CON0 is the contrast at direction 0° and CON45 is the contrast at direction 45°. Resultant reference vectors characteristics for grades G0 to G4 are represented as Eqs. (8).

$$\begin{aligned}
\mathrm{VC(G0)} &= (135, 140, 112, 185, 0.57, 0.39, 0.63, 0.135, 0.11),\\
\mathrm{VC(G1)} &= (147, 150, 112, 85, 0.18, 0.29, 0.79, 0.3, 0.215),\\
\mathrm{VC(G2)} &= (157, 143, 108, 24, 0.32, 0.32, 0.79, 0.16, 0.12),\\
\mathrm{VC(G3)} &= (160, 140, 112, 24, 0.36, 0.34, 0.87, 0.135, 0.11),\\
\mathrm{VC(G4)} &= (153, 143, 121, 60, 0.33, 0.33, 0.7, 0.24, 0.16).
\end{aligned} \quad (8)$$

The values in the same VC have different orders of magnitude, the first three components of VC have the same order of magnitude and their values were much bigger than the last five values of the same vector. This is due to the difference of origins of those components. A normalization process was first applied to the first three components as described in Eq. (9).

$$\mathrm{PS}_N(i,j) = \mathrm{PS}(i,j)/\mathrm{Max}(\mathrm{PS}(i,j)), \quad (9)$$

where PS_N is the normalized PS component, i is the frequency at which the PS is selected (i = 19, 80, or

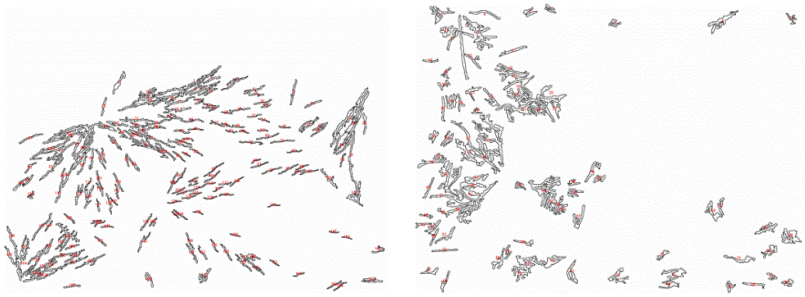

G0 G1

Fig. 8. Line segments in the images for grades 0 and 1.

190), $j = 0, \ldots, 4$ and Max represents the maximum value among PS(i, j).

A normalization process was also applied on the fourth component of the vector, similar to the ones of Eq. (9). The VC was split into three parts in order to provide different weights for components coming from different sources.

The vector became $\mathrm{VC} = \alpha\mathrm{VC}_{\mathrm{PS}} + \beta\mathrm{VC}_{\mathrm{L}} + \gamma\mathrm{VC}_{\mathrm{TA}}$, where, $\mathrm{VC}_{\mathrm{PS}}$ is the first three components related to the normalized PS, VC_{L} included the normalized NBL, and $\mathrm{VC}_{\mathrm{TA}}$ included the last five components related to texture analysis. α, β and γ are weights given to each of the three sub-vectors in order to balance the contribution between them. After experimental testing, the values of the optimal values of the weights are: $\alpha = 35\%$, $\beta = 15\%$, and $\gamma = 50\%$.

$$\mathrm{VC(G0)} = \alpha\mathrm{VC}_{\mathrm{PS}}(\mathrm{G0}) + \beta\mathrm{VC}_{\mathrm{L}}(\mathrm{G0}) + \gamma\mathrm{VC}_{\mathrm{TA}}(\mathrm{G0}), \quad (10)$$

where, $\mathrm{VC}_{\mathrm{PS}}(\mathrm{G0}) = (135/160, 140/160,$ and $112/160)$, $\mathrm{VC}_{\mathrm{L}} = (189/189)$, and $\mathrm{VC}_{\mathrm{TA}}(\mathrm{G0}) = (0.57, 0.39, 0.63, 0.135$ and $0.11)$. The same process was applied to the characteristic vectors of the other images grades in order to get their normalized VCs.

4. Discussion

Development of an objective grading scale for the TF test will support the validity of this test to be applied in the clinic during the routine eye examination, in order to evaluate the ocular tear film, and support the treatment of dry eye disease.

Two major issues are critical for the classification: the construction of feature vectors of the image, and the classification algorithm used to assign a grade to each new image. Characteristic vector construction is the key base of the efficiency of the classification algorithm. In order to develop a competitive algorithm for classification, it is essential to find a set of features with significant and consistent discriminating power. The construction of the VC for each TF image is a combination of three techniques: first, texture features; second, PS analysis; and third, linear shapes determination. Because of scale dependency of texture, its feature extraction is a difficult problem.

Human visual processing uses oriented shapes of the spatial organization to identify shapes. This feature was used in the construction of our vector in order to take into account the linear shapes existing in our TF images which vary from one image grade to the other.

The data presented above suggests that the three main observation aspects confirmed the differentiation between the graded images. This work proposes the method of transforming the visual aspects of the grading of TF into quantitative measurements. The quantities are represented in five characteristics vectors, each vector representing a grade in the recently developed grading scale.[20] The proposed quantification approach is the first of its kind for TF grading. It constitutes the backbone of computer-based grading method in the new grading scale. Some advantages of the computer-based grading approach are expected over the subjective one. It is independent from subjective human judgments which could vary from one to another depending on the skill and experience of the examiner, and it is based on a fixed scale or standard. This approach proposes VCs for each grading point. Extra steps need to be developed in order to make the process completely automatic. Further research is needed in order to find the optimal measurement tool to be used for comparing a VC of a new TF image with those of the new grading scale stored in the database. Weighted Euclidian distance, neural network classification or fuzzy clustering technics need to be explored on simulated and real data. Following this, a classification of the new image relative of the recently developed five-point scale will be possible.

5. Conclusion

This work provides the most important steps toward an automatic objective grading scale of TF images. The resulted vectors characteristics, for each of the grades of the new five-point scale images, are clearly distinct from each other, and they serve as references for the ungraded images of new patients. Our future work is to complete the automation of the grading process of the dry eye from TF images. Distance for measurement should first be developed, taking into account the weighting between the components in the vector and then, a test for a large number of patients, and lastly compared to the manual classification of an expert. A software package will be developed, in order to facilitate the use in the clinics, and to train students on the use of TF in dry eye diagnosis.

Conflict of interest statement

None declared.

Acknowledgments

The authors extend their appreciation to the College of Applied Medical Sciences Research Centre and the Deanship of Scientific Research at King Saud University for its funding for this research.

References

1. M. M. Jumblatt, R. W. McKenzie, P. S. Steele, C. G. Emberts, J. E. Jumblatt, "MUC7 expression in the human lacrimal gland and conjunctiva," *Cornea* **22**, 41–45 (2003).
2. M. B. Abelson, G. Ousler 3rd, "The pros and cons of dry-eye test," *Rev. Opthalmol.* **7**, 62–65 (2011).
3. M. B. Abelson, G. Ousler 3rd, L. A. Nally, T. B. Emory, "Dry eye syndromes: Diagnosis, clinical trials and pharmaceutical treatment–improving clinical trials," *Adv. Exp. Med. Biol.* **506**, 1079–1086 (2002).
4. C. Kent, "Dry eye diagnosis: 21st–Century tools," *Rev. Ophthalmol.* **13**, 28–41 (2013).
5. G. Savini, P. Prabhawsat, T. Kojima, M. Grueterich, E. Espana, E. Goto, "The challenge of dry eye diagnosis," *Clin. Ophthalmol.* **2**, 31–55 (2008).
6. A. Masmali, T. A. Alqahtani, A. Alharbi, G. A. El-Hiti, "Comparative study of repeatability of phenol red thread test versus Schirmer's test in normal adults in Saudi Arabia," *Eye Contact Lens* **40**, 127–131 (2014).
7. J. E. Rose, M. H. Roepke, "An acidified antigen for detection of nonspecific reactions in the plate-agglutination test for bovine brucellosis," *Am. J. Vet. Res.* **18**, 550–555 (1957).
8. M. A. Lemp, "Breakup of the tear film," *Int. Ophthalmol. Clin.* **13**, 97–102 (1973).
9. J. M. Tiffany, "Surface tension in tears," *Arch. Soc. Esp. Ophthalmol.* **81**, 363–366 (2006).
10. M. A. Lemp, A. J. Bron, C. Baudouin, J. M. Benítez Del Castilo, D. Geffen, J. Tauber, G. N. Foulks, J. S. Pepose, D. Sullivan, "Tear osmolarity in the diagnosis and management of dry eye disease," *Am. J. Ophthalmol.* **151**, 792–799 (2011).
11. E. Szalai, A. Berta, Z. Szekanecz, G. Szûcs, L. Módis, "Evaluation of tear osmolarity in non-Sjögren and Sjögren syndrome dry eye patients with the TearLab system," *Cornea* **31**, 867–871 (2012).
12. A. Masmali, S. Alrabiah, A. Alharbi, G. A. El-Hiti, T. Almubrad, "Investigation of tear osmolarity using the TearLab^{TM} osmolarity system in normal adults in Saudi Arabia," *Eye Contact Lens* **40**, 74–78 (2014).
13. K. F. Tabbara, M. Okumoto, "Ocular ferning test. A qualitative test for mucus deficiency," *Ophthalmology* **89**, 712–714 (1982).
14. M. Maragou, E. Vaikousis, A. Ntre, N. Koronis, P. Georgiou, M. Hatzidimitriou, F. Sotsiou, P. Dantis, "Tear and saliva ferning tests in Sjogren's syndrome (SS)," *Clin. Rheumatol.* **15**, 125–132 (1996).
15. M. Rolando, "Tear mucus ferning test in normal and keratoconjunctivitis sicca eyes," *Chibret Int. J. Ophthalmol.* **2**, 32–41 (1984).
16. M. Norn, "Quantitative tear ferning. Clinical investigations," *Acta Ophthalmol.* **72**, 369–372 (1994).
17. E. Vaikoussis, P. Georgiou, D. Nomicarios, "Tear mucus ferning in patients with Sjogren's syndrome," *Doc. Ophthalmol.* **87**, 145–151 (1994).
18. S. Srinivasan, E. Joyce, L. W. Jones, "Tear osmolarity and ferning patterns in postmenopausal women," *Optom. Vis. Sci.* **84**, 588–592 (2007).
19. C. Pensyl, S. Dillehay, "The repeatability of tear mucus ferning grading," *Optom. Vis. Sci.* **745**, 600–604 (1998).
20. A. M. Masmali, P. J. Murphy, C. Purslow, "Development of a new grading scale for tear ferning," *Cont. Lens Anterior Eye* **37**, 178–184 (2014).
21. M. H. Bharati, J. Liu, J. F. MacGregor, "Image texture analysis: Methods and comparisons," *Chemometrics Intell. Lab.* **72**, 57–71 (2004).
22. J. Zhang, T. Tan, "Brief review of invariant texture analysis methods," *Pattern Recogn.* **35**, 735–747 (2002).
23. J. Y. Tou, Y. H. Tay, P. Y. Lau, "Recent trends in texture classification: A review, *Proc. Symp. Progress in Information and Communication Technology (SPICT 2009)*," Kuala Lumpur, Malaysia, pp. 63–68 (2009).
24. B. V. Ramana Reddy, A. Suresh, M. Radhika Mani, V. Vijaya Kumar, "Classification of textures based on features extracted from preprocessing images on Random windows," *Int. J. Adv. Sci. Tech.* **9**, 9–17 (2009).
25. R. M. K. Haralick, K. Shanmugam, I. Dinstein, "Textural features for image classification," *IEEE Trans. Syst. Man. Cybern.* **SMC-3**, 610–621 (1973).
26. R. M. Haralick, "Statistical and structural approaches to texture," *Proc. IEEE* **67**, 786–804 (1979).
27. M. Gipp, G. Marcus, N. Harder, A. Suratanee, K. Rohr, R. König, R. Männer, "Haralick's texture features computed by GPUs for biological applications," **36**, 36109 (2009).
28. L. M. Carey, T. A. Matyas, L. E. Oke, "Evaluation of impaired fingertip texture discrimination and

wrist position sense in patients affected by stroke: Comparison of clinical and new quantitative measures," *J. Hand Ther.* **15**, 71–82 (2002).
29. Y. Rubner, J. Puzicha, C. Tomasi, J. M. Buhmann, "Empirical evaluation of dissimilarity measures for color and texture," *Comput Vis Image Underst* **84**, 25–43 (2001).
30. T. Ojala, M. Pietikäinen, T. Maenpää, "Multiresolution gray-scale and rotation invariant texture classification with local binary patterns," *IEEE T. Pattern Anal.* **24**, 735–743 (2002).
31. V. Bino Sebastian, A. Unnikrishnan, K. Balakrishnan, "Grey level co-occurrence matrices: Generalization and some new features," *Int. J. Comput. Sci.* **2**, 151–157 (2012).
32. V. A. Kovalev, M. Petrou, "Multidimensional co-occurrence matrices for object recognition and matching," *Graph. Models Image Process.* **58**, 187–197 (1996).
33. K. Hammouche, J.-G. Postaire, "Multidimensional texture analysis for unsupervised pattern classification," in *Pattern Recognition Techniques, Technology and Applications*, Chap. 7, P.-Y. Yin, Ed., pp. 163–196, I-Tech, Vienna, Austria (2008).
34. T. Dacheng, L. Xuelong, Y. Yuan, Y. Nenghai, L. Zhengkai, T. Xiao-ou, "A set of novel textural features based on 3D co-occurrence matrix for content-based image retrieval," *Proc. Fifth International Conference on Information Fusion*, Vol. 2, pp. 1403–1407 (2002).
35. A. Oliva, A. B. Torralba, A. Guerin-Dugue, J. Herault, "Global semantic classification of scenes using power spectrum templates," *Challenge of Image Retrieval (CIR99)*, BCS Electronic Workshops in Computing Series, pp. 1–11, Springer Verlag Newcastle, UK (1999).
36. L. Wang, D.-C. He, "Texture classification using texture spectrum," *Pattern Recogn.* **23**, 905–910 (1990).
37. D.-J. Lee, T. F. Krile, S. Mitra, "Power spectrum and spectrum techniques applied to image registration," *Appl. Opt.* **27**, 1099–1106 (1988).